Engineered Tug-of-War Between Kinesin and Dynein Controls Direction of Microtubule Based Transport *In Vivo*

Karim Rezaul[1], Dipika Gupta[1], Irina Semenova[1], Kazuho Ikeda[1,2], Pavel Kraikivski[3], Ji Yu[1], Ann Cowan[1], Ilya Zaliapin[4] and Vladimir Rodionov[1]*

[1]R.D.Berlin Center for Cell Analysis and Modeling, and Department of Cell Biology, UConn Health, 400 Farmington Avenue, Farmington, CT 06030-6406, USA

[2]Current address: Quantitative Biology Center, RIKEN, Osaka 565-0874, Japan

[3]Department of Biological Sciences, Virginia Polytechnic Institute and State University, Blacksburg, VA 24061-0406, USA

[4]Department of Mathematics and Statistics, University of Nevada-Reno, Reno, NV 89557, USA

*Corresponding author: Vladimir Rodionov, rodionov@nso.uchc.edu.

Abstract

Bidirectional transport of membrane organelles along microtubules (MTs) is driven by plus-end directed kinesins and minus-end directed dynein bound to the same cargo. Activities of opposing MT motors produce bidirectional movement of membrane organelles and cytoplasmic particles along MT transport tracks. Directionality of MT-based transport might be controlled by a protein complex that determines which motor type is active at any given moment of time, or determined by the outcome of a tug-of-war between MT motors dragging cargo organelles in opposite directions. However, evidence in support of each mechanisms of regulation is based mostly on the results of theoretical analyses or indirect experimental data. Here, we test whether the direction of movement of membrane organelles *in vivo* can be controlled by the tug-of-war between opposing MT motors alone, by attaching a large number of kinesin-1 motors to organelles transported by dynein to minus-ends of MTs. We find that recruitment of kinesin significantly reduces the length and velocity of minus-end-directed dynein-dependent MT runs, leading to a reversal of the overall direction of dynein-driven organelles *in vivo*. Therefore, in the absence of external regulators tug-of-war between opposing MT motors alone is sufficient to determine the directionality of MT transport *in vivo*.

Keywords dynein, intracellular transport, kinesin, melanophore, pigment granule

Transport of intracellular particles and organelles along cytoplasmic MTs employs molecular motors that drive cargo either toward the MT plus (kinesins) or minus (dynein) end (1). Activities of opposing MT motors produce bidirectional movement of membrane organelles and cytoplasmic particles along MT transport tracks (2–6). Switching between plus- and minus-end directed cargo runs that defines net direction of movement is tightly regulated in cells but the mechanisms of regulation has remained a mystery for decades.

It has been hypothesized that regulation of switching between cargo runs in opposite directions requires a co-ordination complex involving structural and regulatory proteins that dictate which competing MT motor is engaged in motility at any given moment of time (7,8). However, the protein composition of such a co-ordination complex and specific molecular mechanisms underlying motor co-ordination remain unclear. It has also been proposed that regulation of cargo runs in opposite directions is determined by the outcome of a tug-of-war between opposing MT motors. Theoretical studies indicate that bidirectional movement driven by teams of plus- and minus-end directed motors bound to the same cargo follows from the transport properties on individual MT motor proteins measured in single molecule experiments

(9). Small changes in the number of active motors in the teams are predicted to have a significant effect on the net direction of cargo movement (9,10). Circumstantial experimental evidence supports the idea that opposing MT motors are engaged in a tug-of-war in cells, and that the direction of cargo movement along MTs is determined by the relative numbers of active MT motors involved in the competition. Reversal of movement of endosomes in *Dictyostelium* cells or mitochondria in dendrites of neurons was shown to be preceded by a decrease in the velocity of movement, and shape changes that were consistent with simultaneous application of forces by opposing MT motors (11,12). Moreover, in mammalian cells experimentally induced targeting of kinesin-1 or dynein to mostly immotile peroxisomes caused their redistribution to the cell periphery or the cell center, respectively (13,14), and binding of dynein to endosomes in fungal cells correlated with changes in direction of their movement (15). However, experimental data in support of the tug-of-war model for regulation of MT transport are largely indirect, and in some systems, such as *Drosophila* embryos, experimental measurements and theoretical analyses of MT motility suggest that control over direction of MT transport cannot be explained solely by antagonistic activities of kinesin and dynein motors, and requires external regulation that co-ordinates these activities (8,16–18). Inconsistencies in experimental data may be explained by the differences in experimental systems used for analysis of MT-based transport. However, it remains largely unknown whether *in vivo* direction of cargo transport along MTs can be determined by the outcome of a tug-of-war between opposing motors alone.

The tug-of-war model for regulation of MT transport can be directly tested by experimental manipulation of activities of MT motors involved in motility. A simple prediction of the tug-of-war model is that inhibition of one competing MT motor should improve transport in the opposite direction. Acute inhibition of dynein activity indeed caused an increase in anterograde transport of lysosomes in mammalian cells (19). However, this effect was only temporary, and in most cases knockdown or inhibition of activity of one motor generally stopped MT transport in both directions [the so-called 'paradox of codependence' (2)], which made the results of loss of function experiments non-informative. Therefore, to further test regulation of

MT transport through a tug-of-war between opposing MT motors *in vivo* we used a complementary approach and asked whether an acute increase in activity of one MT motor would reduce motility generated by an active competitor leading to a reversal of MT transport direction.

For these experiments, we used *Xenopus* melanophores, which represent an ideal system for studying co-ordinated MT transport. In these cells, fast and synchronous redistribution of thousands of pigment granules either uniformly throughout the cytoplasm or toward the cell center (20), is driven by kinesin-2 [for pigment dispersion (21)] or cytoplasmic dynein [for pigment aggregation (22)] and globally regulated by signaling events. Dispersion signals suppress activity of dynein and activate kinesin-2, resulting in an increase of plus-end runs and eventually in redistribution of pigment granules throughout the cytoplasm. Aggregation signals inhibit kinesin-2 and boost activity of cytoplasmic dynein as evidenced from a decrease of plus-end runs and sudden and dramatic increase of minus-end runs of pigment granules (23,24). Sharp reciprocal changes of MT motor activities induced by pigment aggregation and dispersion signals make *Xenopus* melanophores an ideal experimental system for answering the question whether a tug-of-war alone is sufficient to determine directionality of MT transport *in vivo*. To recreate the tug-of-war situation between opposing MT motors we recruited exogenous constitutively active kinesin to pigment granules. We examined whether this recruitment would affect minus-end directed motility of pigment granules generated by dynein motors activated by pigment aggregation signals, and reverse the net direction of granule movement.

Results and Discussion

To bind kinesin to the surface of pigment granules, we used an inducible FKBP-rapalog-FRB heterodimerization system that takes advantage of the strong interaction between FKBP and FRB protein domains in the presence of the cell-permeable rapamycin analog AP21967 (rapalog) (25). This approach involves coexpression of a motor protein fused with FRB, and a protein specific for a membrane organelle tagged with FKBP (13,26). To identify expressing cells, FRB and FKBP domains were fused to fluorescent proteins EGFP and mCherry, respectively. We chose to target to pigment granules a truncated kinesin-1 that

Table 1: Mass-spectrometry of preparations of pigment granules

| Accession number	Gene name	Protein description	MW	pI	Mean SC	Relative SC
Q7ZYE8	tyrp1	Tyrosinase-related protein 1	60 845	5.33	72	0.0126984
E7FIE3	pmel17	Melanocyte protein Pmel 17	76 488	4.38	26	0.0045193
A1L3E3	gpnmb	Glycoprotein (transmembrane) nmb precursor	65 526	8.1	15	0.0026455
Q3KPL4	NA	Predicted: dopachrome tautomerase (Dct/TYRP2)	58 052	5.98	8	0.0014179
Q5VKN7	tyr	Tyrosinase	28 881	5.2	7	0.0012346
Q7SY95	cd63	CD63	25 758	7.37	6	0.0010582
Q566F3	slc45a2	Solute carrier family 45, member 2	60 310	6.32	4	0.0007055
Q640Z0	bloc1s1	Biogenesis of lysosomal organelles complex-1, subunit 1	14 270	8.89	3	0.0005291
Q0IHH8	gpr143	G protein-coupled receptor 143	45 197	8.28	2	0.0003527

contained dimerization and motor domains but lacked the helical tail domain (13) making it constitutively active in MT gliding but insensitive to regulation by the pigment aggregation signaling pathway.

To identify an abundant pigment granule protein suitable for recruitment of kinesin-1 in amounts sufficient to compete with granule-associated dynein, we performed quantitative mass spectrometry of preparations of isolated pigment granules. The pigment granule preparations contained multiple proteins known to be involved in biogenesis of pigment granules or synthesis of the pigment melanin (Table 1). The most abundant pigment granule protein was tyrosinase-related protein-1 (TYRP1),

an enzyme involved in melanin biosynthesis (27). This transmembrane protein has a short cytoplasmic domain suitable for attaching kinesin-1 (27). To find out how the levels of TYRP1 bound to pigment granules compared with the levels of dynein or kinesin, we performed quantitative immunoblotting of preparations of pigment granules with antibodies raised against the cytoplasmic domain of TYRP1, dynein intermediate chain or kinesin-1 A subunit (Figures 1A and S1). We determined the number of molecules of MT motor proteins and TYRP1 in granule preparations used for immunoblotting, and divided these numbers by the number of pigment granules in these preparations. This quantitative analysis showed that each pigment granule contained approximately 700–800
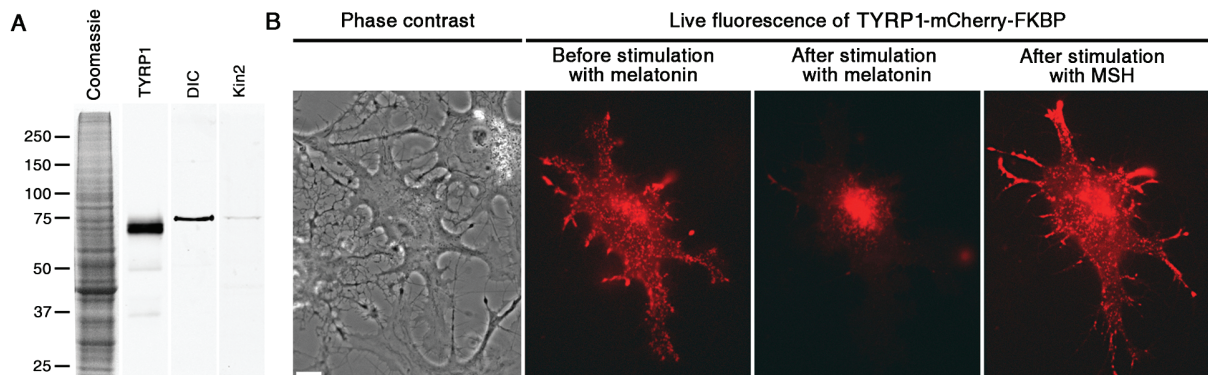
Figure 1: TYRP1 binds pigment granules in melanophores. A) Immunoblots of preparations of pigment granules probed with antibodies against TYRP1 or subunits of motor proteins involved in pigment granule transport; coomassie-stained gel of a preparation of pigment granules (left), immunoblots of pigment granule preparations with antibodies raised against TYRP1 (middle left), dynein intermediate chain (DIC; middle right), and A subunit of kinesin-2 (kin2; right). B) Phase contrast (left) and fluorescence images of a pigment-free melanophore expressing TYRP1-FKBP-mCherry before (middle left) or after (middle right) stimulation with melatonin, or subsequent treatment with MSH (right); TRP-mCherry-FKBP is localized to fluorescent dots that accumulate in the cell center or disperse throughout the cytoplasm after treatment of cells with melatonin and MSH, respectively, as would be expected for pigment granules. Scale bar, 5 μm.

TYRP1-mCherry-FKBP   Kinesin-1-EGFP-FRB

- Rapalog

+ Rapalog
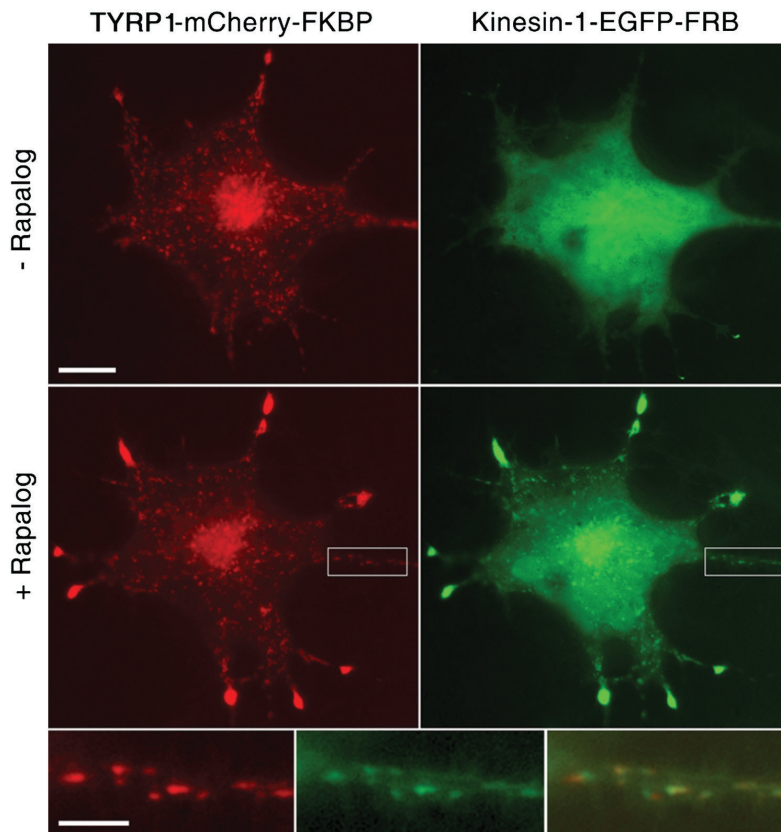
Figure 2: Rapalog treatment recruits kinesin-1-EGFP-FRB to the pigment granules that bound TYRP1-FKBP-mCherry. Top and middle, fluorescence images of melanophores coexpressing TYRP1-FKBP-mCherry (left) and kinesin-1-EGFP-RB (right) before (top) or after (middle) stimulation with rapalog; bottom, high magnification images (left and middle) and overlay (right) of boxed areas shown in low magnification images. Treatment of melanophores with rapalog leads to acquisition of EGFP fluorescence by the mCherry positive dots, indicating that kinesin-1-EGFP- FRB binds pigment granules. Scale bars, 5 µm (top) and 2 µm (bottom).

molecules of TYRP1, $\sim$50–60 molecules of dynein and $\sim$20–30 molecules of kinesin-2. We concluded that TYRP1 was a far more abundant granule protein than the MT motors involved in granule transport, suggesting that exogenous TYRP1 overexpressed in melanophores will incorporate into pigment granules at levels exceeding the levels of cytoplasmic dynein. Consequently, binding of kinesin-1 to the cytoplasmic domain of exogenous TYRP1 would be expected to result in a molar excess of kinesin-1 over dynein on the granule surface. Thus, loading of kinesin-1 onto pigment granules through coexpression of kinesin-1-EGFP-FRB and TYRP1-FKBP-mCherry should significantly increase the active kinesin to active dynein ratio during pigment aggregation.

TYRP1-FKBP-mCherry expressed in melanophores was expected to incorporate in the pigment granule membrane, and in the presence of rapalog recruit kinesin-1-EGFP-FRB. To test whether TYRP1-FKBP-mCherry was associated with pigment granules, we expressed this construct in melanophores depleted of pigment, produced by supplementing the tissue culture

medium with the tyrosinase inhibitor phenylthiourea (PTU). Pigment-free cells were used because the melanin core of pigment granules interferes with fluorescence microscopy. We found that in pigment-free melanophores TYRP1-FKBP-mCherry fluorescence was associated with dots that aggregated in the cell center or redispersed throughout the cytoplasm in response to treatment with melatonin or melanocyte-stimulating hormone (MSH), respectively, as would be expected for pigment granules (Figure 1B). We also found that treatment of cells coexpressing TYRP1-FKBP-mCherry and kinesin-1-EGFP-FRB with rapalog led to accumulation of EGFP fluorescence by mCherry-positive dots (Figure 2), consistent with recruitment of kinesin-1-EGFP-FRB to pigment granules. Rapalog treatment also caused redistribution of the fluorescent dots into the tips of cell processes (Figure 2), that was likely explained by the plus-end directed MT transport of pigment granules driven by the recruited kinesin-1 (28). We conclude that TYRP1-FKBP-mCherry bound to pigment granules and in the presence of rapalog recruited kinesin-1-EGFP-FRB that moved granules along MTs toward the cell periphery.

We performed control experiments to determine whether binding of TYRP1-FKBP-mCherry to pigment granules was specific, and whether rapalog treatment induced recruitment of kinesin-1-EGFP-FRB through selective interaction with FRB. We found that TYRP1-FKBP-mCherry did not localize to other membrane organelles, such as mitochondria, visualized by fluorescence staining with MitoTracker Deep Red (Figure S2A). Furthermore, treatment with rapalog of melanophores coexpressing kinesin-1-EGFP-FRB- and TYRP1-FKBP-mCherry did not cause redistribution of mitochondria to the cell periphery, whereas pigment granules, as expected, accumulated at the cell margin (Figure S2B). We also found that TYRP1-FKBP-mCherry did not bind to peroxisomes that were revealed by coexpression of GFP-tagged peroxisomal protein Pex26 (Figure S3A). Moreover, treatment with rapalog of melanophores with aggregated pigment granules coexpressing kinesin-1-EGFP-FRB and Pex3-mRFP-FKBP, known to selectively bind to peroxisomes (13), led to their accumulation at the cell edge (Figure S3B, left) while pigment granules remained clustered in the pigment aggregate located in the cell center (Figure S3B, right). Taken together, the results of control experiments showed that in melanophores coexpressing kinesin-1-EGFP-FRB and TYRP1-FKBP-mCherry rapalog treatment selectively targeted kinesin-1 to pigment granules.

We estimated the level of kinesin-1 recruited to pigment granules by comparing GFP fluorescence of individual pigment granules in rapalog-treated cells, to fluorescence of single kinesin-1-EGFP-FRB molecules detected in these cells with TIRF microscopy. These measurements showed that each pigment granule bound on average 401 ± 211 molecules of kinesin-1-EGFP-FRB. Given that each pigment granule bound $\sim 50-60$ molecules of dynein, we concluded that total force produced by granule-bound kinesin-1 motors should significantly exceed the force generated by dyneins. Therefore recruitment of kinesin-1 would be expected to interfere with dynein-dependent motility of pigment granules. To determine whether such interference indeed takes place, we induced pigment aggregation with melatonin in rapalog-treated melanophores coexpressing kinesin-1-EGFP-FRB and TYRP1-FKBP-mCherry and observed granule movement. Cells that were not treated with rapalog served as

a control. To facilitate detection of single pigment granules, we used melanophores incubated overnight in tissue culture medium lacking PTU. After a short incubation in a PTU-free medium, cells started to produce melanin in a fraction of pigment granules. The sparse population of pigment granules containing melanin facilitated their detection and recording using conventional phase contrast microscopy. We found that, as expected, control cells responded to melatonin treatment by a rapid (~ 15 min) accumulation of pigment granules in the cell center (Figure 3, top, and Movie S1). In marked contrast to control cells, in the rapalog-treated melanophores stimulated with melatonin pigment granules remained scattered throughout the cytoplasm and enriched in the cell processes, but never aggregated in the cell center (Figure 3, bottom, and Movie S2). An increase in the length of treatment of cells with melatonin to 1 h did not change the peripheral distribution of pigment granules (Movie S2). This result clearly shows that recruitment of kinesin-1 to the pigment granules inhibited their dynein-driven net displacement toward the cell center.

Inhibition of dynein-dependent aggregation of pigment caused by the recruitment of kinesin-1 could be explained by a global decrease in granule motility and/or stimulation of plus-end directed transport through an increase in plus-end runs, a decrease in minus-end runs or both. To get insight into the mechanism of inhibition of pigment granule aggregation caused by recruitment of kinesin-1, we recorded and tracked individual pigment granules, and used movement trajectories to determine fractions of immotile granules, and statistics of bidirectional granule movement in control and rapalog-treated cells exposed to pigment aggregation stimuli. To facilitate recording of single pigment granules, we once again used cells with reduced numbers of melanin-containing pigment granules that we obtained by overnight incubation of pigment-free melanophores in the absence of PTU to initiate melanin biosynthesis. We recorded 15 s time-lapse image sequences of single pigment granules in these cells after coexpression of kinesin-1-EGFP-FRB and TYRP1-FKBP-mCherry and treatment with melatonin in the presence or absence of rapalog. We found that fractions of stationary pigment granules (that shifted position during 15 s period of observation for distances $\leq 0.5 \,\mu m$, an average granule diameter) were similar between control and
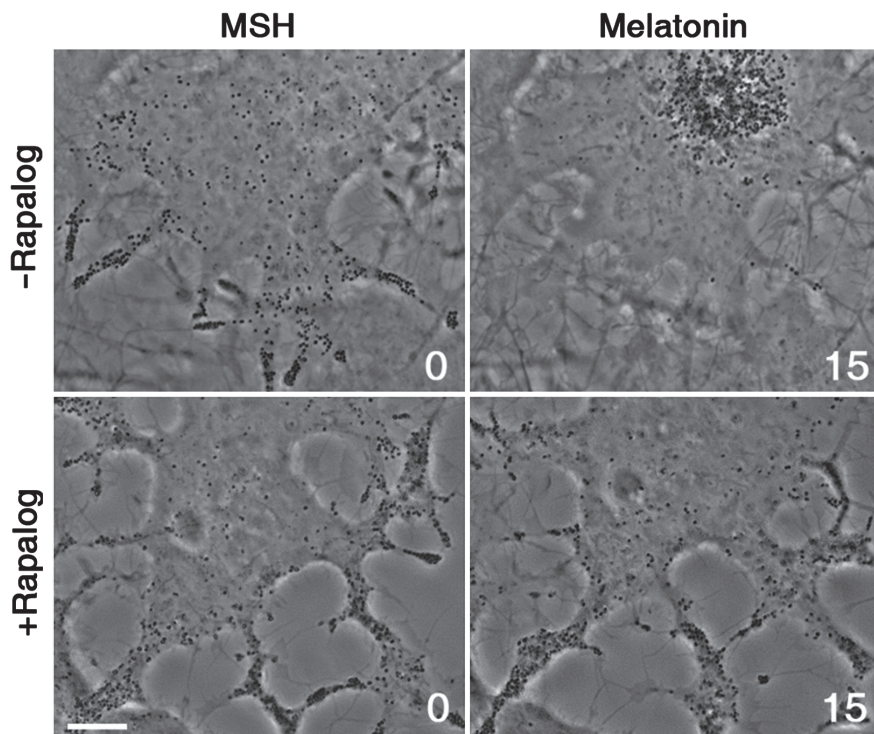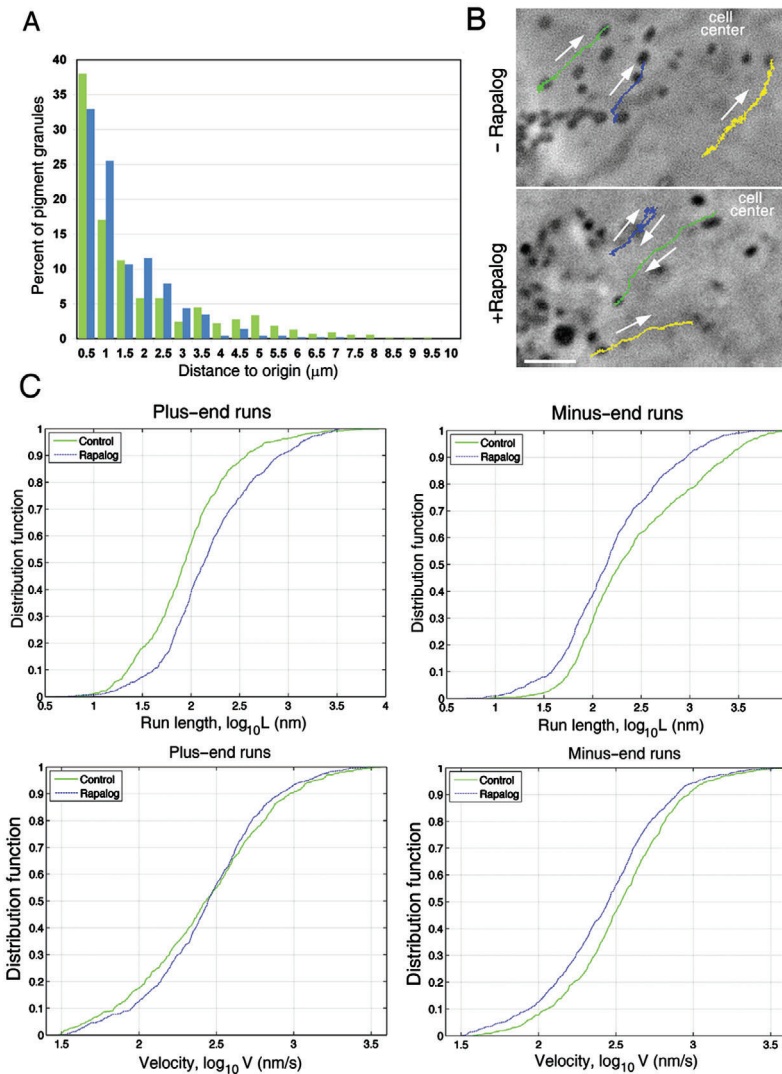
Figure 3: Recruitment of kinesin-1 inhibits accumulation of pigment granules in the cell center induced by pigment aggregation signals. Phase contrast images of melanophores coexpressing kinesin-1-EGFP-FRB and TYRP1-FKBP-mCherry treated with MSH (left images) or melatonin (right images) in the absence (top row) or presence (bottom row) of rapalog; rapalog treatment that recruits kinesin-1 to pigment granules inhibits their aggregation in the cell center. Numbers indicate time in minutes. Scale bar, 5 μm.

rapalog-treated melanophores (∼38% and ∼33%, respectively). Net displacement for short distances (1–3 μm) was slightly increased in expense of displacement for long distances in the case of rapalog-treated melanophores but this effect was not dramatic and could result from a change in the pattern of bidirectional movement in the presence of rapalog (see below) that would be expected to decrease net displacement of pigment granules from the starting point. We concluded that recruitment of kinesin-1 did not induce global inhibition of pigment granule motility. We found, however, that the patterns of granule motility were significantly different in control and rapalog-treated melanophores. In control cells, pigment granules made long runs directed to the cell center that were infrequently interrupted by either short runs in the opposite direction or pauses (Figure 4B, top, and Movie S3). In contrast to control cells, in rapalog-treated melanophores pigment granules made long runs in both directions (Figure 4B, bottom, and Movie S4). To quantify the effect of rapalog treatment on bidirectional granule transport, we decomposed granule trajectories into runs in the plus- and minus-end direction, and pauses, and compared granule movement statistics in control and rapalog-treated cells. We calculated the average values for velocities and lengths of uninterrupted granule runs in

opposite directions (Table 2) and generated cumulative distribution functions for these parameters that showed the probabilities of movement of pigment granules for defined distances or with defined velocities to the plus- or minus-ends of MTs (Figure 4C). We found that, as expected, rapalog treatment stimulated plus-end directed motility of pigment granules by increasing the length of plus-end directed runs as evidenced from a shift in the distribution function to larger values (Figure 4C, left, top) and a rise in the average run length (Table 2). However, the velocity of plus-end runs did not change significantly (Figure 4C, left, bottom; Table 2), consistent with the results of *in vitro* work indicating that at high loads kinesins-2 (that generates plus-end runs in control cells) and kinesin-1 (largely responsible for plus-end runs in rapalog-treated melanophores) move along MTs with similar velocities (29). Remarkably, we found that rapalog treatment shifted to lower values distribution functions for lengths and velocities of minus-end runs (Figure 4C, right) and reduced their average values to ∼44% and ∼82% of control levels (Table 2). These data show that recruitment of kinesin-1 after treatment of melanophores with rapalog significantly suppressed minus-end directed motility of pigment granules produced by dynein.

Figure 4: Recruitment of kinesin-1-EGFP-FRB does not inhibit motility of pigment granules but enhances their plus-end directed movement by increasing the length of plus-end runs and reducing the length and velocity of minus-end runs. A) Frequency histogram of distances traveled by pigment granules in control (green) or rapalog-treated (blue) cells within 15 s time interval used for recoding of the granule motility; in control cells, pigment granules more frequently travel for longer distances compared to rapalog-treated cells, but rapalog treatment does not increase the fraction of essentially immotile granules that traveled for distances not exceeding 0.5 μm (average diameter of pigment granules), — an indication that recruitment of kinesin-1 does not block pigment granule motility. B) Motility tracks of pigment granules in control (top) or rapalog-treated (bottom) melanophores coexpressing kinesin-1-EGFP- FRB and TYRP1-FKBP-mCherry and stimulated with melatonin. Rapalog treatment increases the frequency and length of granule runs directed away from the cell center (upper right corner of each image). Color-coded lines indicate tracks of individual granules. Arrows indicate direction of granule movement. Numbers indicate time in minutes. Scale bar, 2 μm. C) Cumulative distribution function plots that show the probability distribution for lengths (top) or velocities (bottom) of plus-end (left) or minus-end (right) granule runs in control (green) or rapalog-treated (blue) cells coexpressing kinesin-1-EGFP- FRB and TYRP1-FKBP-mCherry; recruitment of kinesin-1-EGFP-FRB increases the probability of longer plus-end granule runs (upper left) without changing the probability distribution of their velocities (lower left), and at the same time increases the probabilities of shorter and slower minus-end runs (upper right and lower right, respectively), — an indication that kinesin-1 interferes with dynein motility.

Table 2: Parameters of MT-based movement of pigment granules during pigment granule aggregation in melanophores coexpressing TYRP1-FKBP-mCherry and Kinesin-1-GFP-FRB in the absence or in the presence of rapalog

Movement parameters	−Rapalog	+Rapalog
Velocity of minus-end runs (nm/s)	471.4 ± 16.4	388.9 ± 14.1
Length of minus-end runs (nm)	783.1 ± 48.7	348.1 ± 20.9
Velocity of plus-end runs (nm/s)	430.8 ± 19.0	397.1 ± 13.7
Length of plus-end runs (nm)	208.8 ± 21.8	326.9 ± 17.7
Duration of pauses (s)	1.1 ± 0.1	1.1 ± 0.1
Number of analyzed pigment granules	138	133
Number of analyzed cells	23	21

To determine whether stimulation of plus-end directed and suppression of minus-end directed motility of pigment granules caused by recruitment of kinesin-1 was sufficient to reverse the net direction of pigment granule transport, we applied rapalog to kinesin-1-EGFP-FRB- and TYRP1-FKBP-mCherry-coexpressing melanophores whose pigment granules were preaggregated with melatonin. We found that rapalog treatment induced gradual dispersion of pigment granules (Figure 5 and Movie S5). We concluded that kinesin-1 bound to pigment granules overpowered dynein, and reversed the net direction of pigment granule transport.

In this study, we showed that loading of pigment granules with constitutively active kinesin-1 overruled the effects of global transport signals and induced reversal of the direction of transport produced by cytoplasmic dynein. We believe that this reversal is explained by the defeat of dynein by kinesin-1 in a tug-of-war. First, activity of kinesin-1 that was targeted to pigment granules in our study could not be modulated by a co-ordination complex because kinesin-1 is not involved in redistribution of pigment granules in *Xenopus* melanophores (21) and lacks the C-terminal region that is generally responsible for the regulation of motor protein activity (30). Second, our data show that kinesin-1 was recruited to pigment granules at levels exceeding the levels of endogenous dynein and therefore was expected to win the competition. Finally, changes in parameters of minus-end directed movement of pigment granules induced by kinesin-1 attachment measured in our work are consistent with predictions made by studies that explained bidirectional MT transport by a continuous tug-of-war between opposing MT motors

(9,10). We believe that sporadic interactions of multiple granule-bound kinesin-1 motors with MTs generated drag force sufficient to rip dynein motors off MTs, thereby shortening minus-end-directed MT granule runs, and applied breaks on moving dynein motors leading to a decrease in their velocity. Indeed, *in vitro* optical trapping experiments showed that a team of dynein motors adapts to applied load by generating larger forces but reducing velocity of movement along MTs (31). Taken together, our data indicate that the outcome of a tug-of-war between opposing MT motors alone can determine the direction of long-range MT-based transport of membrane organelles in cells.

Our data show that an experimentally induced increase in the number of kinesin-1 motors bound to pigment granules reverses direction of their transport along MTs generated by dynein motors that are fully activated by pigment aggregation signals. While our work does not address the question about the specific mechanisms controlling MT transport in the melanophores that we used as an experimental system, we believe that results of our experiments have a general importance because they validate that regulation of MT transport can occur by control over the outcome of a tug-of-war between opposing MT motors alone. Results of numerous studies indicate that intracellular signals may indeed affect the levels of MT motors associated with membrane organelles by posttranslational modifications of MT motor proteins themselves and/or adaptor and scaffolding proteins involved in their attachment to cargo (30,32–34). Therefore the manipulation of the outcome of a tug-of-war between MT motors of opposite polarity recapitulated in our study may be a general mechanism for regulating the direction of MT transport. However, in some cells, including melanophores, the direction of MT transport may be controlled by a complementary mechanism that involves co-ordinating activities of opposing MT motors and thus eliminating the tug-of-war between them (8,16,18). Understanding mechanisms of co-ordinated regulation of opposing MT motors that prevents a tug-of-war is an exciting line of future investigation.

Materials and Methods

Cell culture

Permanent cell lines of *Xenopus laevis* melanophores were cultured as described previously (35). To deplete cells of melanin, tissue culture
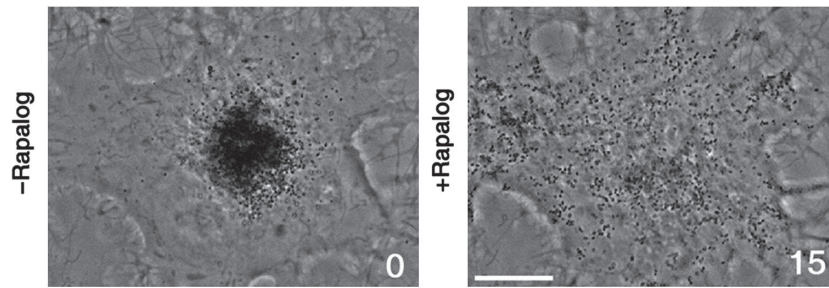
Figure 5: **Recruitment of kinesin-1 reverses direction of pigment granule transport induced by pigment aggregation signals.** Phase contrast images of a cell coexpressing kinesin-1-EGFP- FRB and TYRP1-FKBP-mCherry treated with melatonin to aggregate pigment granules before (left) or after (right) treatment with rapalog; rapalog-induced recruitment of kinesin-1 leads to dispersion of pigment granules, and therefore reverses direction of their dynein-dependent movement. Numbers indicate time in minutes. Scale bar, 5 μm.

medium was supplemented with 1 mM PTU. Aggregation or dispersion of pigment granules was induced by treatment of cells with melatonin or MSH, respectively (35).

Mass-spectrometry analysis of pigment granule proteins

For mass-spectrometry analysis of granule proteins, pigment granules were purified using sucrose gradient centrifugation as described previously (36). Tryptic digests of granule proteins were analyzed using liquid chromatography tandem mass spectrometry (LC-MS/MS), and all MS/MS spectra were searched against the *Xenopus laevis* database using the SEQUEST algorithm for protein identification. A label-free quantitative method, spectral counting, was applied to estimate protein abundance as described in Ref 37.

Expression vectors for TYRP1-FKBP-mCherry, Kinesin-1-EGFP-FRB and Pex3-mRFP-FKBP

To generate an expression vector containing TYRP1-FKBP-mCherry, *Xenopus laevis* TYRP1 cDNA (GenBank BC43815; I.M.A.G.E. clone MXL1736-8950383 obtained from Thermo Scientific) was amplified by PCR and cloned into an mCherry-N1 expression vector (Clontech) upstream of mCherry tag using the BglII and EcoRI restriction sites. PCR-amplified FKBP DNA was then inserted between the TYRP1 and mCherry DNA sequences using the BamH1 restriction site. Plasmids designed for expression of Kinesin-1-EGFP-FRB, GFP-Pex26 and Pex3-mRFP-FKBP DNA were described previously (13).

Production of polyclonal antibodies against TYRP1

Polyclonal antibodies against TYRP1 were produced by immunization of rabbits with synthetic peptide corresponding to the C-terminal amino acid sequence (LIGESYPRYVEDKQENTQSV) of the *Xenopus laevis* TYRP1, and purified from antisera by affinity chromatography on a column with covalently attached antigen.

Quantitative immunoblotting and quantification of numbers of MT motors and TYRP1 attached to each pigment granule.

For quantitative immunoblotting, pigment granules were isolated as described previously (36), and pigment granule proteins were extracted with a buffer containing 1% TX-100. For quantification of amounts of dynein or kinesin-2 pigment granule proteins were separated using SDS-gel electrophoresis. The amount of TYRP1 was quantified using a dot blot assay because the reference protein sample (conjugate with BSA of a TYRP1 derived peptide that was used for antibody production) separated into multiple bands during SDS electrophoresis, which made quantification of integrated band intensity unreliable. Western blots of SDS gels were incubated with mouse monoclonal antibodies against the intermediate chain of cytoplasmic dynein (DIC; 74.1; Covance) or the A subunit of Kinesin-2 (BD Biosciences). Dot immunoblots of granule proteins were incubated with rabbit monospecific antibodies against *Xenopus* TYRP1-derived peptide. Protein bands or dots were revealed by staining blots with IRDye800-conjugated affinity-purified anti-mouse or anti-rabbit secondary antibodies (Rockland Immunochemicals), and the intensity of the infrared signal was quantified with the Odyssey Infrared Imaging System (Li-Cor Biosciences). All measured integrated intensities of protein bands or dots fell into a linear range.

To determine the numbers of MT motor and TYRP1 molecules in pigment granule preparations, the intensities of signals generated by antibody staining of blots of granule extracts were compared with intensities of signals produced by staining of blots of reference proteins — cytoplasmic dynein isolated from bovine brain and separated from dynactin by MonoQ chromatography (38), recombinant EGFP- and His-tagged kinesin-2 heterodimer expressed in a baculovirus expression system and purified using chromatography on Ni-NTA agarose (39) or a conjugate of TYRP1-derived peptide used for antibody production with bovine serum albumin at a molar ratio of 5:1 (Figure S1). Quantities of proteins in pigment granule preparations were calculated based on molecular masses of cytoplasmic dynein, EGFP-kinesin-2, and TYRP1 ∼ 1.2 mDa, ∼200 kDa, and ∼55 kDa, respectively. Numbers of molecules of dynein, kinesin-2

or TYRP1 in pigment granule preparations were calculated as $N = Q$ [mol] $\times N_A$, where Q [mol] is quantity of a protein in moles, and N_A is the Avogadro constant.

For quantification of the numbers of TYRP1, dynein and kinesin-2 molecules per pigment granule, the number of pigment granules per mL of pigment granule preparation used in immunoblotting experiments was determined using two independent experimental approaches. The first approach involved direct counting of pigment granules in suspension using a hemocytometer. The second approach estimated the number of pigment granules per melanophore by counting them using phase contrast images of well-spread cells. We found that each melanophore contained on average $5718 \pm .436$ pigment granules (mean $\pm$ SEM; $n = 20$). The number of pigment granules per cell was multiplied by the number of cells used for isolation of pigment granules to determine their total amount. The two approaches resulted in similar values for the number of pigment granules per mL of pigment granule preparation ($\sim 3 \times 10^{10}$). The number of molecules of each protein in 1 mL of pigment granule preparation was then divided by the number of pigment granules.

Cell transfection

Cells were transfected using GeneCellin DNA transfection reagent according to instructions provided by the manufacturer.

Fluorescent labeling of mitochondria or peroxisomes

For fluorescent labeling of mitochondria, PTU-treated melanophores were stained for 2–3 min with MitoTracker Deep Red (ThermoFisher) taken at concentration 1 mM. For fluorescent labeling of peroxisomes, we expressed in melanophores GFP-tagged peroxisomal marker protein Pex26 [GFP-Pex26; (13)]. Prior to image acquisition, MitoTracker Deep Red-stained or GFP-Pex26-expressing cells were fixed with 4% formaldehyde for 30 min.

Image acquisition and analysis

Fluorescence images of pigment granules, mitochondria, and peroxisomes were taken with Nikon Eclipse Ti microscope equipped with 100×1.4 NA Plan Apochromat objective, and Andor iXon back-illuminated EM CCD camera driven by Metamorph software.

For measurement of kinesin-1-EGFP-FRB levels on pigment granules, cells were imaged using a modified Olympus IX81 epi-fluorescence microscope with 488 nm laser illumination. To obtain average single-molecule intensity for EGFP chromophore, cells were fixed with 4% formaldehyde. Melanophores with low expression level of kinesin-1-EGFP-FRB were selected, and photobleached until individual diffraction-limited fluorescence spots could be detected at the cell periphery, and exhibited on/off intensity ('blinking') phenomena characteristic of single molecules. Acquired stacks of images were analyzed using a single molecule tracking program, which identifies individual fluorescence spots by locally fitting an image to a 2D Gaussian function (40). Total fluorescence intensity for each spot was computed via numerical integration of the Gaussian fit. To calculate the number of molecules of EGFP per pigment granule, live

images of melanophores were acquired using the same imaging setup. Image acquisition time was reduced twofold to avoid saturation of the camera. Total fluorescence intensity of individual pigment granules (identified based on TYRP1-FKBP-mCherry fluorescence) was quantified after background subtraction by integrating pixel intensity over $1.6 \times 1.6\,\mu m$ area around individual pigment granules. To calculate the number of kinesin-1-EGFP-FRB molecules per pigment granule, integrated fluorescence intensities of pigment granules were divided by expected total intensity of a single EGFP chromophore, and the data were corrected for the difference in acquisition time. A total of 60 pigment granules in four cells were used for analysis.

For the pigment granule tracking, phase contrast images of pigment granules were acquired using a Nikon Eclipse TE300 inverted microscope equipped with a 100×1.25 NA Plan Achromat objective lens, and additional $2.5 \times$ lens placed in front of video camera (35). Time series (15 s long each) of phase contrast images of melanophores were acquired via stream acquisition option of Metamorph at a video rate (30 frames/seconds) 5 min after the treatment of cells with melatonin. Pigment granules were tracked with the particle tracking module of Metamorph software. For comparison of pigment granule motility in control and rapalog-treated cells, all pigment granules in the $12 \times 16\,\mu m$ field of view were tracked and net lengths of their trajectories were measured using the 'distance to origin' function of Metamorph software. For quantification of parameters of bidirectional MT transport, tracking involved only those motile pigment granules that never collided with their neighbors and remained in the focal plane of the microscope during the entire period of observation. Trajectories of pigment granules were decomposed into plus-end runs (directed to the cell periphery), minus-end runs (directed to the cell center) and pauses using the Multiscale Trend Analysis (23). Cumulative distribution functions for lengths and velocities of granule runs were computed as follows:

$$F(x) = \frac{\#\left\{i : x_i \leq x\right\}}{n}$$

where x_i denotes one of the estimated characteristics (run length or velocity) for the i-th run.

Acknowledgments

Supporting Information

Additional Supporting Information may be found in the online version of this article:

Figure S1: Quantification of the amounts of cytoplasmic dynein, kinesin-2 or TYRP1 in pigment granule preparations using

immunoblotting. Images of protein bands separated by SDS-gel electrophoresis (A, B) or protein dots (C) revealed by immunostaining of pigment granule extracts (GE) or preparations of reference proteins, cytoplasmic dynein purified from bovine brain (A; Dyn), recombinant kinesin-2 (B; Kin-2), or BSA conjugated with TYRP1-derived peptide (BSA-TYRP1 peptide conjugate) at a molar ratio 1:5; primary antibodies used for immunostaining were monoclonal antibodies against dynein intermediate chain (A; Dic Ab), kinesin-2 A subunit (B; Kin-2A Ab), or peptide polyclonal antibody against TYRP1 (C; TYRP1 Ab); secondary antibodies were anti-mouse (A, B) or anti-rabbit (C) antibodies conjugated with IRDye800. Comparison of integrated band or dot intensities in cell extracts with normalized band or dot intensities of reference proteins showed that concentrations of dynein, kinesin-2, and TYRP1 in granule extracts were 6, 0.2 and 2 μg/mL.

Figure S2: TYRP1-mCherry-FKBP does not colocalize with mitochondria, and recruitment to pigment granules of kinesin-1-EGFP-FRB does not lead to accumulation of mitochondria at the cell periphery. (A) Top, fluorescence images of a melanophore expressing TYRP1-mCherry FKBP (left) stained with MitoTracker Deep Red (right); bottom, high magnification images (left and middle) and overlay (right) of boxed areas shown in low magnification images; TYRP1-mCherry FKBP does not colocalize with mitochondria. Scale bars, 5 μm (top) /and 1 μm (bottom). (B) distribution of pigment granules and mitochondria in a cell coexpressing TYRP1-mCherry FKBP and kinesin-1-EGFP-FRB treated with rapalog and stained with MitoTracker Deep Red; rapalog treatment caused recruitment of Kinesin-1-EGFP-FRB (not shown) to TYRP1-mCherry FKBP-positive pigment granules (left) leading to their concentration at the cell margin, but does not induce peripheral accumulation of mitochondria stained with MitoTracker Deep Red (right). Scale bar, 10 μm.

Figure S3: TYRP1-mCherry FKBP does not bind to peroxisomes, and recruitment kinesin to peroxisomes does not induce redistribution of pigment granules to the cell periphery. (A) Top, fluorescence images of a melanophore coexpressing TYRP1-mCherry FKBP (left) and peroxisome marker GFP-Pex26 (right); bottom, high magnification images (left and middle) and overlay (right) of boxed areas shown in low magnification images; TYRP1-mCherry FKBP does not bind to peroxisomes; Scale bars, 5 μm (top) and 2 μm (bottom). (B) Fluorescence (left) and phase contrast (right) images of a melanophore with aggregated pigment granules coexpressing FKBP-and mRFP-tagged peroxisome marker Pex3-mRFP-FKBP, and kinesin-1-EGFP-FRB before (top) or after (bottom) treatment with rapalog; rapalog treatment caused recruitment of kinesin-1-EGFP-FRB (not shown) to Pex3-mRFP-FKBP-positive peroxisomes (left) leading to their accumulation at the cell margin but did not induce dispersion of pigment granules that remained clustered in the pigment aggregate located in the center of the cell (right); Scale bar, 10 μm.

Movie S1: Time-lapse phase contrast images of a control melanophore coexpressing TYRP1-FKBP-mCherry and kinesin-1-EGFP-FRB that was stimulated with melatonin without pretreatment with rapalog. Stimulation with melatonin induced rapid aggregation of pigment granules in the cell center. Numbers indicate time in minutes:seconds; scale bar, 5 μm. This movie corresponds to images shown in Figure 3 (top).

Movie S2: Time-lapse phase contrast images of a melanophore coexpressing TYRP1-FKBP-mCherry and kinesin-1-EGFP-FRB that was treated with rapalog and stimulated with melatonin. Pigment granules did not respond to melatonin treatment by aggregating in the cell center but instead remained dispersed throughout the cytoplasm. Numbers indicate time in minutes:seconds; scale bar, 5 μm. This movie corresponds to images shown in Figure 3 (bottom).

Movie S3: Time-lapse high magnification phase contrast images of a control melanophore coexpressing TYRP1-FKBP-mCherry and kinesin-1-EGFP-FRB that was stimulated with melatonin without pretreatment with rapalog. Most pigment granules move in the direction of the cell center (upper right corner in the movie). Color-coded lines indicate tracks of three individual pigment granules. Numbers indicate time in seconds; scale bar, 2 μm. This movie corresponds to the image shown in Figure 4B (top).

Movie S4: Time-lapse high magnification phase contrast images of a melanophore coexpressing TYRP1-FKBP-mCherry and kinesin-1-EGFP-FRB that was treated with rapalog and stimulated with melatonin. Color-coded lines indicate tracks of three individual pigment granules that move in the direction of the cell center (upper right corner in the movie; yellow line), to the cell periphery (green line) or reverse direction of movement after initial displacement to the cell center (blue line). Numbers indicate time in seconds; scale bar, 2 μm. This movie corresponds to the image shown in Figure 4B (bottom).

Movie S5: Time-lapse phase contrast images of a melanophore coexpressing TYRP1-FKBP-mCherry and kinesin-1-EGFP- FRB pretreated with melatonin for aggregation of pigment granules, and treated with rapalog. Rapalog treatment induced dispersion of pigment granules. Numbers indicate time in minutes:seconds; scale bar, 5 μm. This movie corresponds to images shown in Figure 5.

References

1. Vale RD. The molecular motor toolbox for intracellular transport. Cell 2003;112:467–480.
2. Hancock WO. Bidirectional cargo transport: moving beyond tug of war. Nat Rev Mol Cell Biol 2014;15:615–628.
3. Jolly AL, Gelfand VI. Bidirectional intracellular transport: utility and mechanism. Biochem Soc Trans 2011;39:1126–1130.
4. Gross SP. Hither and yon: a review of bi-directional microtubule-based transport. Phys Biol 2004;1:R1–R11.
5. Welte MA. Bidirectional transport along microtubules. Curr Biol 2004;14:R525–R537.
6. Blehm BH, Selvin PR. Single-molecule fluorescence and in vivo optical traps: how multiple dyneins and kinesins interact. Chem Rev 2014;114:3335–3352.
7. Gross SP, Welte MA, Block SM, Wieschaus EF. Coordination of opposite-polarity microtubule motors. J Cell Biol 2002;156:715–724.
8. Gross SP, Welte MA, Block SM, Wieschaus EF. Dynein-mediated cargo transport in vivo: a switch controls travel distance. J Cell Biol 2000;148:945–956.
9. Muller MJ, Klumpp S, Lipowsky R. Tug-of-war as a cooperative mechanism for bidirectional cargo transport by molecular motors. Proc Natl Acad Sci USA 2008;105:4609–4614.

10. Hendricks AG, Perlson E, Ross JL, Schroeder HW 3rd, Tokito M, Holzbaur EL. Motor coordination via a tug-of-war mechanism drives bidirectional vesicle transport. Curr Biol 2010;20:697–702.

11. Soppina V, Rai AK, Ramaiya AJ, Barak P, Mallik R. Tug-of-war between dissimilar teams of microtubule motors regulates transport and fission of endosomes. Proc Natl Acad Sci USA 2009;106:19381–19386.

12. Gennerich A, Schild D. Finite-particle tracking reveals submicroscopic-size changes of mitochondria during transport in mitral cell dendrites. Phys Biol 2006;3:45–53.

13. Kapitein LC, Schlager MA, van der Zwan WA, Wulf PS, Keijzer N, Hoogenraad CC. Probing intracellular motor protein activity using an inducible cargo trafficking assay. Biophys J 2010;99:2143–2152.

14. van Bergeijk P, Adrian M, Hoogenraad CC, Kapitein LC. Optogenetic control of organelle transport and positioning. Nature 2015;518:111–114.

15. Schuster M, Lipowsky R, Assmann MA, Lenz P, Steinberg G. Transient binding of dynein controls bidirectional long-range motility of early endosomes. Proc Natl Acad Sci USA 2011;108:3618–3623.

16. Kunwar A, Tripathy SK, Xu J, Mattson MK, Anand P, Sigua R, Vershinin M, McKenney RJ, Yu CC, Mogilner A, Gross SP. Mechanical stochastic tug-of-war models cannot explain bidirectional lipid-droplet transport. Proc Natl Acad Sci USA 2011;108:18960–18965.

17. Kural C, Kim H, Syed S, Goshima G, Gelfand VI, Selvin PR. Kinesin and dynein move a peroxisome in vivo: a tug-of-war or coordinated movement? Science 2005;308:1469–1472.

18. Welte MA, Gross SP, Postner M, Block SM, Wieschaus EF. Developmental regulation of vesicle transport in Drosophila embryos: forces and kinetics. Cell 1998;92:547–557.

19. Yi JY, Ori-McKenney KM, McKenney RJ, Vershinin M, Gross SP, Vallee RB. High-resolution imaging reveals indirect coordination of opposite motors and a role for LIS1 in high-load axonal transport. J Cell Biol 2011;195:193–201.

20. Nascimento AA, Roland JT, Gelfand VI. Pigment cells: a model for the study of organelle transport. Annu Rev Cell Dev Biol 2003;19:469–491.

21. Tuma MC, Zill A, Le Bot N, Vernos I, Gelfand V. Heterotrimeric kinesin II is the microtubule motor protein responsible for pigment dispersion in Xenopus melanophores. J Cell Biol 1998;143:1547–1558.

22. Nilsson H, Wallin M. Evidence for several roles of dynein in pigment transport in melanophores. Cell Motil Cytoskeleton 1997;38:397–409.

23. Zaliapin I, Semenova I, Kashina A, Rodionov V. Multiscale trend analysis of microtubule transport in melanophores. Biophys J 2005;88:4008–4016.

24. Gross SP, Tuma MC, Deacon SW, Serpinskaya AS, Reilein AR, Gelfand VI. Interactions and regulation of molecular motors in Xenopus melanophores. J Cell Biol 2002;156:855–865.

25. Banaszynski LA, Liu CW, Wandless TJ. Characterization of the FKBP.rapamycin.FRB ternary complex. J Am Chem Soc 2005;127:4715–4721.

26. Kapitein LC, Schlager MA, Kuijpers M, Wulf PS, van Spronsen M, MacKintosh FC, Hoogenraad CC. Mixed microtubules steer dynein-driven cargo transport into dendrites. Curr Biol 2010;20:290–299.

27. del Marmol V, Beermann F. Tyrosinase and related proteins in mammalian pigmentation. FEBS Lett 1996;381:165–168.

28. Kapitein LC, van Bergeijk P, Lipka J, Keijzer N, Wulf PS, Katrukha EA, Akhmanova A, Hoogenraad CC. Myosin-V opposes microtubule-based cargo transport and drives directional motility on cortical actin. Curr Biol 2013;23:828–834.

29. Andreasson JO, Shastry S, Hancock WO, Block SM. The mechanochemical cycle of mammalian kinesin-2 KIF3A/B under load. Curr Biol 2015;25:1166–1175.

30. Verhey KJ, Hammond JW. Traffic control: regulation of kinesin motors. Nat Rev Mol Cell Biol 2009;10:765–777.

31. Rai AK, Rai A, Ramaiya AJ, Jha R, Mallik R. Molecular adaptations allow dynein to generate large collective forces inside cells. Cell 2013;152:172–182.

32. Fu MM, Holzbaur EL. Integrated regulation of motor-driven organelle transport by scaffolding proteins. Trends Cell Biol 2014;24:564–574.

33. Barlan K, Rossow MJ, Gelfand VI. The journey of the organelle: teamwork and regulation in intracellular transport. Curr Opin Cell Biol 2013;25:483–488.

34. Akhmanova A, Hammer JA 3rd. Linking molecular motors to membrane cargo. Curr Opin Cell Biol 2010;22:479–487.

35. Ikeda K, Semenova I, Zhapparova O, Rodionov V. Melanophores for microtubule dynamics and motility assays. Methods Cell Biol 2010;97:401–414.

36. Kashina AS, Semenova IV, Ivanov PA, Potekhina ES, Zaliapin I, Rodionov VI. Protein kinase A, which regulates intracellular transport, forms complexes with molecular motors on organelles. Curr Biol 2004;14:1877–1881.

37. Qendro V, Lundgren DH, Rezaul K, Mahony F, Ferrell N, Bi A, Latifi A, Chowdhury D, Gygi S, Haas W, Wilson L, Murphy M, Han DK. Large-scale proteomic characterization of melanoma expressed proteins reveals nestin and vimentin as biomarkers that can potentially distinguish melanoma subtypes. J Proteome Res 2014;13:5031–5040.

38. Malikov V, Kashina A, Rodionov V. Cytoplasmic dynein nucleates microtubules to organize them into radial arrays in vivo. Mol Biol Cell 2004;15:2742–2749.

39. Schroeder HW 3rd, Hendricks AG, Ikeda K, Shuman H, Rodionov V, Ikebe M, Goldman YE, Holzbaur EL. Force-dependent detachment of kinesin-2 biases track switching at cytoskeletal filament intersections. Biophys J 2012;103:48–58.

40. Niu L, Yu J. Investigating intracellular dynamics of FtsZ cytoskeleton with photoactivation single-molecule tracking. Biophys J 2008;95:2009–2016.